 Bull. Chem. Soc. Jpn. Vol. 79, No. 11, 1729–1741 (2006)

Syntheses, Structures, and O_2-Reactivities of Copper(I) Complexes with Bis(2-pyridylmethyl)amine and Bis(2-quinolylmethyl)amine Tridentate Ligands

Atsushi Kunishita, Takao Osako, Yoshimitsu Tachi, Junji Teraoka,* and Shinobu Itoh*

Departments of Chemistry and Materials Science, Graduate School of Science, Osaka City University, 3-3-138 Sugimoto, Sumiyoshi-ku, Osaka 558-8585

Received May 8, 2006; E-mail: shinobu@sci.osaka-cu.ac.jp

The structure and O_2-reactivity of the copper(I) complexes supported by bis[(6-phenyl-2-pyridyl)methyl]amine tridentate ligands ($L5^R$) and bis(2-quinolylmethyl)amine tridentate ligands ($L6^R$) have been investigated in detail in order to get insights into the steric effects of the tridentate ligands on copper(I)/O_2 chemistry. In the cases of benzyl amine and phenethyl amine derivatives [R = $-CH_2Ph$ (Bz) and $-CH_2CH_2Ph$ (Phe)], the reaction between the ligands and $[Cu^I(CH_3CN)_4]^+$ gave the corresponding copper(I)–acetonitrile complexes having a distorted tetrahedral geometry. On the other hand, the 2,2-diphenylethyl amine derivative $L6^R$ [R = $-CH_2CHPh_2$ (PhePh)] afforded a copper(I) complex without an ancillary ligand (CH_3CN) and having intramolecular d–π interaction between the copper(I) ion and the phenyl group of the alkyl substituent PhePh. The acetonitrile complexes were then converted to the corresponding CO-complexes by reacting with CO gas. The X-ray structures of all CO-complexes have been determined, and the complexes have a similar distorted tetrahedral geometry. In addition, the 6-phenyl group of $L5^R$ imparts a large steric effect on the metal-binding. The CO-complexes were converted to the copper(I) complexes without having any ancillary ligands in order to examine their O_2-reactivity. Significantly large differences in O_2-reactivity were found among the copper(I) complexes. On the basis of O_2-reactivity together with the X-ray structures and the oxidation potentials of the copper(I) complexes, the steric effects of the hetero-aromatic donor groups (6-substituted pyridine and quinoline) as well as the alkyl substituents (R) are discussed in detail.

As a part of our continuing efforts to understand the ligand effects on copper(I)/O_2 chemistry, we have been studying the structure and reactivity of copper(I) complexes supported by a series of tridentate ligands $L1^R$–$L4^R$ (Chart 1).[1] Copper(I) complexes with bis[2-(2-pyridyl)ethyl]amine tridentate ligands $L1^R$ have been shown to afford (μ-η^2:η^2-peroxo)dicopper(II) complexes **A** (Chart 2) from the reaction with O_2 at a low temperature.[1–4] The side-on peroxo dicopper(II) complexes **A** supported by the $L1^R$ ligands have been extensively studied as structural and functional models of oxy-hemocyanin and oxy-tyrosinase due to their ability to reversibly bind dioxygen and hydroxylate aromatic compounds.[5–9] Recently, we have also demonstrated that the use of bis(2-pyridylmethyl)amine tridentate ligand $L3^{Phe}$ [R = $-CH_2CH_2Ph$ (Phe), Chart 1] instead of $L1^R$ induces O–O bond cleavage of the peroxo complex to afford a bis(μ-oxo)dicopper(III) complex **B** under the same reaction conditions.[10] It has been reported that the electron-donor ability of pyridine of the (2-pyridylmethyl)amine ligands, which afford a smaller 5-member chelate ring, is higher than that of the [2-(2-pyridyl)ethyl]amine ligands, which comprise a larger 6-member chelate ring.[11] Thus, the $L3^{Phe}$ ligand with the higher electron-donor ability may enhance O–O bond cleavage of the peroxo species and stabilize the higher oxidation state of the metal center to give the bis(μ-oxo)dicopper(III) complex **B**.

6-Methyl substituent on the pyridine nucleus of $L2^R$ has been demonstrated to cause a decrease in electron-donor ability of the pyridine due to a steric repulsion between the substituent and the metal ion.[12] Thus, the reactivity of copper(I) complex with $L2^{Phe}$, $[Cu^I(L2^{Phe})(MeCN)]^+$ (Phe = $-CH_2CH_2Ph$),

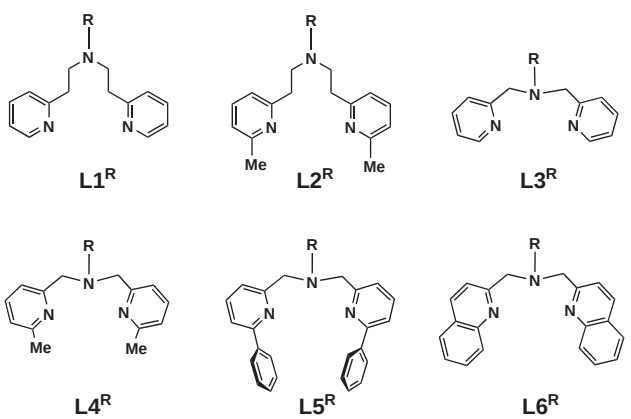

Chart 1.

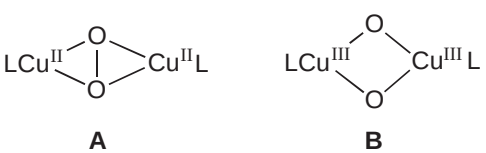

Chart 2.

Published on the web November 9, 2006; doi:10.1246/bcsj.79.1729

toward O_2 is almost lost.[13] In this case, the weaker electron-donor ability of the 6-methylpyridine of $L2^{Phe}$ makes the oxidation potential of copper(I) complex higher as compared to that of the copper(I) complexes with $L1^R$, thus stabilizing the lower oxidation state of copper(I). On the other hand, the introduction of methyl group at C-6 of pyridine of $L3^R$ to give $L4^R$ (Chart 1) resulted in formation of the side-on peroxo complex **A** rather than the bis(μ-oxo) complex **B** in the oxygenation reaction of the copper(I) complexes of $L4^R$.[14] Thus, the introduction of 6-methyl substituent shifted the equilibrium between **A** and **B** toward the peroxo side. In this case as well, the 6-methyl substituent in $L4^R$ decreases the electron-donor ability of pyridine, prohibiting the O–O bond cleavage to give the peroxo complex **A** as the major product.

In this study, the structure and O_2-reactivity of the copper(I) complexes supported by bis[(6-phenyl-2-pyridyl)methyl]amine tridentate ligands $L5^R$ and bis(2-quinolylmethyl)amine tridentate ligands $L6^R$ (Chart 1) have been investigated in detail to understand further the steric effects of the tridentate ligands on copper(I)/O_2 chemistry. Although the structure and reactivity of some copper(I) complexes supported by the tetradentate ligands with 6-phenyl-2-pyridyl and 2-quinolyl donor groups have been reported,[15–17] denticity of the supporting ligands, i.e. tridentate vs tetradentate, has been well documented to cause large effects on the O_2-reactivity of copper(I).[3,4] Thus, this study using the tridentate ligands with the bulky donor groups will give significantly important information about how the ligands control the Cu(I)–O_2 reactivity in the N_3-tridentate ligand systems.

Experimental

General. The reagents and the solvents used in this study, except the ligands and the copper complexes, were purchased with the highest available purity and were further purified using the standard methods, if necessary.[18] *N*,*N*-Bis(2-pyridylmethyl)-benzylamine ($L3^{Bz}$) and *N*,*N*-bis(2-quinolylmethyl)benzylamine ($L6^{Bz}$) were prepared by the reported procedures.[19,20] *N*,*N*-Bis(2-quinolylmethyl)-2-phenethylamine ($L6^{Phe}$) and *N*,*N*-bis(2-quinolylmethyl)-2,2-diphenylethylamine ($L6^{PhePh}$) were obtained from the previous study.[21] FT-IR spectra were recorded on a Jasco FTIR-4100, and UV–visible spectra were taken on a Jasco V-570 or a Hewlett Packard 8453 photo diode array spectrophotometer equipped with a Unisoku thermostated cell holder designed for low-temperature measurements (USP-203). ^{1}H NMR spectra were recorded on a JEOL FT-NMR Lambda 300WB or a JEOL FT-NMR GX-400 spectrometer. ESR spectra were recorded on a JEOL JES-FE2XG spectrometer at -150 °C. Mass spectra were recorded on a JEOL JMS-700T Tandem MS-station mass spectrometer. ESI–MS (electrospray ionization mass spectra) measurements were performed on a PE SCIEX API 150EX. Raman scattering was excited by a He/Cd laser (Kinmon Electrics, CDR80SG) and an Ar laser (NEC GLG3300), and the resonance Raman light was dispersed with a JEOL 400D Raman spectrometer equipped with a modified cryostat cell holder USP-203 for the Raman measurements. Cyclic voltammetric measurements were performed on an ALS-630A electrochemical analyzer in deaerated CH_3CN containing 0.10 M NBu_4PF_6 as a supporting electrolyte. The Pt working electrode (BAS) was polished with BAS polishing alumina suspension and rinsed with acetone before use. The counter electrode was a platinum wire. The measured potentials were recorded with respect to an $Ag/AgNO_3$ (0.01 M) reference electrode. All electrochemical measurements were carried out in a glovebox filled with Ar gas at 25 °C. Elemental analyses were recorded with a Perkin-Elmer or a Fisons instruments EA1108 Elemental Analyzer.

Synthesis. *N*,*N*-Bis[(6-phenyl-2-pyridyl)methyl]benzylamine ($L5^{Bz}$): To a methanol solution (40 mL) containing benzylamine (702 mg, 6.5 mmol) and 6-phenyl-2-pyridinecarboxaldehyde (2.4 g, 13.0 mmol)[22] was added acetic acid slowly to adjust the pH of the solution to 4, and the mixture was stirred for 1 h at room temperature. $NaBH_3CN$ (806 mg, 13.0 mmol) was then added slowly to the solution, and the mixture was stirred at room temperature for 3 days. After the reaction, the mixture was acidified to pH 1 by adding conc. HCl while cooling with an ice bath. Removal of the solvent by evaporation gave an oily material, which was dissolved into an NaOH aqueous solution (pH 14). The aqueous solution was then extracted with $CHCl_3$ (40 mL × 5), and the combined organic layer was dried over Na_2SO_4. After removal of Na_2SO_4 by filtration, evaporation of the solvent gave a brown material, from which $L5^{Bz}$ was isolated as an oily material by silica-gel column chromatography (eluent: hexane:AcOEt = 6:1) in a 50% yield (1.5 g); ^{1}H NMR ($CDCl_3$, 400 MHz) δ 3.81 (2H, s, –C*H*$_2$–), 3.96 (4H, s, –C*H*$_2$–N–C*H*$_2$–), 7.24 (1H, t, J = 8.0 Hz), 7.30–7.51 (10H, m), 7.59 (4H, dd, J = 3.6 and 7.6 Hz), 7.73 (2H, t, J = 7.6 Hz), 8.00 (4H, br d, J = 7.6 Hz); HRMS (FAB$^+$) m/z = 442.2271, calcd for $C_{31}H_{28}N_3$ = 442.2283.

***N*,*N*-Bis[(6-phenyl-2-pyridyl)methyl]-2-phenethylamine ($L5^{Phe}$):** This compound was prepared by following the same procedures as described for $L5^{Bz}$ using phenethylamine instead of benzylamine in a 49% yield. ^{1}H NMR ($CDCl_3$, 400 MHz) δ 2.94 (4H, s, –C*H*$_2$C*H*$_2$–), 4.03 (4H, s, –C*H*$_2$–N–C*H*$_2$–), 7.13–7.27 (5H, m), 7.36 (2H, d, J = 7.6 Hz), 7.40 (2H, d, J = 7.2 Hz), 7.45 (4H, t, J = 7.2 Hz), 7.56 (2H, d, J = 8.0 Hz), 7.65 (2H, t, J = 7.8 Hz), 8.00 (4H, br d, J = 8.0 Hz); HRMS (FAB$^+$) m/z = 456.2441, calcd for $C_{32}H_{30}N_3$ = 456.2440.

Caution: The perchlorate salts used in this study are all potentially explosive and should be handled with care.

[Cu^I($L3^{Bz}$)(CH_3CN)]PF_6 (3^{Bz}·CH_3CN): Ligand $L3^{Bz}$ (144.7 mg, 0.5 mmol) was treated with an equimolar amount of [Cu^I-(CH_3CN)$_4$]PF_6 (186.2 mg, 0.5 mmol) in CH_3CN (2 mL) under Ar atmosphere in a glovebox. After stirring the mixture for 5 min at room temperature, an insoluble material was removed by filtration. Addition of ether (100 mL) to the filtrate caused a pale yellow powder to precipitate upon standing for several minutes. The supernatant was then removed by decantation, and the remaining pale yellow solid was washed three times with ether and dried to give complex **3^{Bz}·CH_3CN** in a 60% yield. ^{1}H NMR (CD_3CN, 400 MHz) δ 1.91 (3H, s, C*H*$_3$CN), 3.79 (4H, s, –C*H*$_2$–N–C*H*$_2$–), 3.84 (2H, s, –C*H*$_2$–), 7.18–7.32 (5H, m), 7.32–7.43 (4H, m), 7.77 (2H, dt, J = 1.6 and 8.0 Hz), 8.51 (2H, d, J = 4.8 Hz); FT-IR (KBr) 835 cm^{-1} (PF_6^-); HRMS (FAB$^+$): m/z 352.0871, calcd for $C_{19}H_{19}CuN_3$ 352.0875; Anal. Calcd for [Cu^I($L3^{Bz}$)(CH_3CN)]PF_6·H_2O ($C_{21}H_{24}CuF_6N_4OP$): C, 45.29; H, 4.34; N, 10.06%. Found: C, 45.25; H, 4.05; N, 10.10%.

[Cu^I($L3^{Bz}$)(CO)]PF_6 (3^{Bz}·CO): (107.7 mg, 0.2 mmol) was suspended into EtOH (5 mL) under CO atmosphere. After stirring the mixture for 30 min at -40 °C, insoluble material was removed by filtration. Addition of ether (100 mL) to the filtrate caused a pale white powder to precipitate upon standing for several minutes. The supernatant was then removed by decantation, and the white solid was washed three times with ether and dried to give complex **3^{Bz}·CO** in a 73% yield. Micro crystals of **3^{Bz}·CO**

were obtained by liquid–liquid phase diffusion of ether into a CH_3CN solution of the complex. FT-IR (KBr) 2091 cm^{-1} (C=O), 835 cm^{-1} (PF_6^-); HRMS (FAB^+): m/z 352.0878, calcd for $C_{19}H_{19}CuN_3$ 352.0875; Anal. Calcd for $[Cu^I(L3^{Bz})(CO)]PF_6$-$(C_{20}H_{19}CuF_6N_3OP)$: C, 45.68; H, 3.64; N, 7.99%. Found: C, 45.31; H, 3.61; N, 7.89%.

$[Cu^I(L5^{Bz})(CH_3CN)]ClO_4$ (5^{Bz}•CH_3CN): This compound was prepared by following the same procedures as described for **3^{Bz}•CH_3CN** using $L5^{Bz}$ (132.3 mg, 0.3 mmol) and $[Cu^I(CH_3$-$CN)_4]ClO_4$ instead of $L3^{Bz}$ and $[Cu^I(CH_3CN)_4]PF_6$, respectively. In this case, CH_2Cl_2 (4 mL) was used as the solvent instead of CH_3CN, and the solid product was obtained by adding *n*-hexane to the filtrate. The yield was 87%. ^1H NMR (CD_2Cl_2, 400 MHz) δ 1.73 (3H, br s, C*H*$_3$CN), 3.96 (2H, br s, –N–C*H*$_2$–), 4.06 (4H, br s, –C*H*$_2$–N–C*H*$_2$–), 7.20–7.35 (11H, m), 7.44 (2H, t, $J = 7.4$ Hz), 7.49–7.58 (6H, m), 7.85 (2H, t, $J = 8.0$ Hz); FT-IR (KBr) 1092 and 621 cm^{-1} (ClO_4^-); HRMS (FAB^+): m/z 504.1501, calcd for $C_{31}H_{27}CuN_3$ 504.1501; Anal. Calcd for $[Cu^I(L5^{Bz})$-$(CH_3CN)]ClO_4 \cdot 1.5H_2O$ ($C_{33}H_{33}ClCuN_4O_{5.5}$): C, 58.93; H, 4.95; N, 8.33%. Found: C, 58.69; H, 4.58; N, 8.49%.

$[Cu^I(L5^{Bz})(CO)]ClO_4$ (5^{Bz}•CO): This compound was prepared in a similar manner as described for the synthesis of **3^{Bz}•CO** by using **5^{Bz}•CH_3CN** (73.0 mg, 0.11 mmol) instead of **3^{Bz}•CH_3CN** as a white powder in an 81% yield. Micro crystals of **5^{Bz}•CO** were obtained by diffusion of *n*-hexane into a CH_2Cl_2 solution of the complex. FT-IR (KBr) 2098 and 2088 cm^{-1} (C=O), 1091 and 622 cm^{-1} (ClO_4^-); HRMS (FAB^+): m/z 532.1442, calcd for $C_{32}H_{27}CuN_3O$ 532.1450; Anal. Calcd for $[Cu^I(L5^{Bz})$-$(CO)]ClO_4$ ($C_{32}H_{27}ClCuN_3O_5$): C, 60.76; H, 4.30; N, 6.64%. Found: C, 60.64; H, 4.21; N, 6.52%.

$[Cu^I(L5^{Bz})]ClO_4$ (5^{Bz}): This complex was prepared by removing CO from **5^{Bz}•CO**. Thus, a methanol solution of the CO-complex was heated on an oil bath at 70 °C for 30 min, and then the solvent was removed under reduced pressure to give a yellow oily material of **5^{Bz}** in a 95% yield. FT-IR (KBr) 1083 and 623 cm^{-1} (ClO_4^-); HRMS (FAB^+): m/z 504.1495, calcd for $C_{31}H_{27}CuN_3$ 504.1501.

$[Cu^I(L5^{Phe})(CH_3CN)]ClO_4$ (5^{Phe}•CH_3CN): This compound was prepared by following the same procedures as described for **3^{Bz}•CH_3CN** using $L5^{Phe}$ (91.2 mg, 0.2 mmol) and $[Cu^I(CH_3$-$CN)_4]ClO_4$ instead of $L3^{Bz}$ and $[Cu^I(CH_3CN)_4]PF_6$, respectively, in a 51% yield. ^1H NMR (CD_2Cl_2, 400 MHz) δ 1.85 (3H, s, C*H*$_3$-CN), 2.90 (2H, t, $J = 7.4$ Hz, –NCH$_2$C*H*$_2$–), 3.08 (2H, t, $J = 7.4$ Hz, –NC*H*$_2$CH$_2$–), 4.10 (4H, br, –C*H*$_2$–N–C*H*$_2$–), 6.85 (1H, t, $J =$ 7.0 Hz), 7.00–7.09 (3H, m), 7.28 (5H, t, $J = 8.0$ Hz), 7.40 (2H, d, $J = 8.0$ Hz), 7.45–7.51 (6H, m), 7.55 (2H, d, $J = 7.6$ Hz), 7.90 (2H, t, $J = 8.0$ Hz); FT-IR (KBr) 1092 and 623 cm^{-1} (ClO_4^-); HRMS (FAB^+): m/z 518.1643, calcd for $C_{32}H_{29}CuN_3$ 518.1657; Anal. Calcd for $[Cu^I(L5^{Phe})(CH_3CN)]ClO_4$ ($C_{34}H_{32}ClCuN_4O_4$): C, 61.91; H, 4.89; N, 8.49%. Found: C, 61.71; H, 4.79; N, 8.27%.

$[Cu^I(L5^{Phe})(CO)]ClO_4$ (5^{Phe}•CO): This complex was prepared in a similar manner as described for the synthesis of **3^{Bz}•CO** by using **5^{Phe}•CH_3CN** (100.0 mg, 0.15 mmol) instead of **3^{Bz}•CH_3CN** as a white powder in a 79% yield. Micro crystals of **5^{Phe}•CO** were obtained by diffusion of *n*-hexane into a CH_2Cl_2 solution of the complex. FT-IR (KBr) 2102 and 2092 cm^{-1} (C=O), 1092 and 622 cm^{-1} (ClO_4^-); HRMS (FAB^+): m/z 546.1588, calcd for $C_{33}H_{29}CuN_3O$ 546.1606; Anal. Calcd for $[Cu^I(L5^{phe})(CO)]$-ClO_4 ($C_{33}H_{29}ClCuN_3O_5$): C, 61.30; H, 4.52; N, 6.50%. Found: C, 61.10; H, 4.44; N, 6.52%.

$[Cu^I(L5^{Phe})]ClO_4$ (5^{Phe}): This complex was prepared in a similar manner as described for the synthesis of **5^{Bz}** using **5^{Phe}•CO** instead of **5^{Bz}•CO** in a 96% yield. Micro crystals of **5^{Phe}** were obtained by vapor diffusion of ether into a CH_2Cl_2 solution of the complex. FT-IR (KBr) 1116 and 621 cm^{-1} (ClO_4^-); HRMS (FAB^+): m/z 518.1656, calcd for $C_{32}H_{29}CuN_3$ 518.1658; Anal. Calcd for $[Cu^I(L5^{Phe})]ClO_4 \cdot 2/3H_2O$ ($C_{32}H_{30.333}ClCuN_3$-$O_{4.666}$): C, 60.95; H, 4.85; N, 6.66%. Found: C, 60.81; H, 4.88; N, 6.44%.

$[Cu^I(L6^{Bz})(CH_3CN)]ClO_4$ (6^{Bz}•CH_3CN): This compound was prepared by following the same procedures as described for **3^{Bz}•CH_3CN** using $L6^{Bz}$ (117.0 mg, 0.3 mmol) and $[Cu^I(CH_3$-$CN)_4]ClO_4$ instead of $L3^{Bz}$ and $[Cu^I(CH_3CN)_4]PF_6$, respectively, in an 80% yield. ^1H NMR (CD_2Cl_2, 400 MHz) δ 2.19 (3H, s, C*H*$_3$-CN), 4.02 (2H, d, $J = 16.0$ Hz, –NCH*H*–), 4.11 (2H, s, –C*H*$_2$–), 4.33 (2H, d, $J = 16.0$ Hz, –NC*H*H–), 7.24 (3H, d, $J = 6.4$ Hz), 7.38 (3H, d, $J = 8.4$ Hz), 7.45 (1H, d, $J = 5.6$ Hz), 7.65 (2H, t, $J = 8.4$ Hz), 7.92 (4H, t, $J = 8.4$ Hz), 8.29 (2H, d, $J = 8.4$ Hz), 8.53 (2H, d, $J = 8.4$ Hz); FT-IR (KBr) 1093 and 620 cm^{-1} (ClO_4^-); HRMS (FAB^+): m/z 452.1191, calcd for $C_{27}H_{23}CuN_3$ 452.1188; Anal. Calcd for $[Cu^I(L6^{Bz})(CH_3CN)]ClO_4 \cdot 0.5H_2O$ ($C_{29}H_{27}ClCuN_4O_{4.5}$): C, 57.81; H, 4.52; N, 9.30%. Found: C, 58.07; H, 4.39; N, 9.21%.

$[Cu^I(L6^{Bz})(CO)]ClO_4$ (6^{Bz}•CO): This complex was prepared in a similar manner as described for the synthesis of **3^{Bz}•CO** by using **6^{Bz}•CH_3CN** (119.0 mg, 0.2 mmol) instead of **3^{Bz}•CH_3CN** as a white powder in an 89% yield. Micro crystals of **6^{Bz}•CO** were obtained by diffusion of *n*-hexane into a CH_2Cl_2 solution of the complex. FT-IR (KBr) 2088 cm^{-1} (C=O), 1089 and 621 cm^{-1} (ClO_4^-); HRMS (FAB^+): m/z 452.1184, calcd for $C_{27}H_{23}$-CuN_3 452.1188; Anal. Calcd for $[Cu^I(L6^{Bz})(CO)]ClO_4$ ($C_{28}H_{23}$-$ClCuN_3O_5$): C, 57.93; H, 3.99; N, 7.24%. Found: C, 57.90; H, 3.90; N, 7.09%.

$[Cu^I(L6^{Bz})]ClO_4$ (6^{Bz}): This complex was prepared in a similar manner as described for the synthesis of **5^{Bz}** using **6^{Bz}•CO** instead of **5^{Bz}•CO** as a yellow oily material in a 95% yield. FT-IR (KBr) 1091 and 621 cm^{-1} (ClO_4^-); HRMS (FAB^+): m/z 452.1185, calcd for $C_{27}H_{23}CuN_3$ 452.1188.

$[Cu^I(L6^{Phe})(CH_3CN)]ClO_4$ (6^{Phe}•CH_3CN): This compound was prepared by following the same procedures as described for **3^{Bz}•CH_3CN** using $L6^{Phe}$ (321.0 mg, 0.8 mmol) and $[Cu^I(CH_3$-$CN)_4]ClO_4$ instead of $L3^{Bz}$ and $[Cu^I(CH_3CN)_4]PF_6$, respectively, in an 86% yield. ^1H NMR (CD_2Cl_2, 400 MHz) δ 2.24 (3H, s, C*H*$_3$CN), 2.92–3.09 (2H, m, –NCH$_2$C*H*$_2$Ph), 3.20–3.38 (2H, m, –NC*H*$_2$CH$_2$Ph), 4.16 (2H, d, $J = 16.0$ Hz, –NCH*H*–), 4.42 (2H, d, $J = 16.0$ Hz, –NCH*H*–), 7.07–7.20 (2H, m), 7.20–7.34 (3H, m), 7.43–7.55 (2H, m), 7.62–7.75 (2H, m), 7.88–8.06 (4H, m), 8.34 (2H, d, $J = 8.3$ Hz), 8.51 (2H, d, $J = 8.6$ Hz); FT-IR (KBr) 1109, 1090, and 625 cm^{-1} (ClO_4^-); HRMS (FAB^+): m/z 466.1347, calcd for $C_{28}H_{25}CuN_3$ 466.1345; Anal. Calcd for $[Cu^I(L6^{Phe})$-$(CH_3CN)]ClO_4$ ($C_{30}H_{28}ClCuN_4O_4$): C, 59.31; H, 4.65; N, 9.22%. Found: C, 58.99; H, 4.74; N, 9.00%.

$[Cu^I(L6^{Phe})(CO)]ClO_4$ (6^{Phe}•CO): This complex was prepared in a similar manner as described for the synthesis of **3^{Bz}•CO** by using **6^{Phe}•CH_3CN** (285.0 mg, 0.47 mmol) instead of **3^{Bz}•CH_3CN** as a white powder in an 84% yield. Micro crystals of **6^{Phe}•CO** were obtained by liquid–liquid phase diffusion of *n*-hexane into a CH_2Cl_2 solution of the complex. FT-IR (KBr) 2101 cm^{-1} (C=O), 1091 and 622 cm^{-1} (ClO_4^-); HRMS (FAB^+): m/z 466.1344, calcd for $C_{28}H_{25}CuN_3$ 466.1345; Anal. Calcd for $[Cu^I(L6^{phe})(CO)]ClO_4$ ($C_{29}H_{25}ClCuN_3O_5$): C, 58.59; H, 4.24; N, 7.07%. Found: C, 58.42; H, 4.25; N, 6.97%.

$[Cu^I(L6^{Phe})]ClO_4$ (6^{Phe}): This complex was prepared in a similar manner as described for the synthesis of **5^{Bz}** using

6^{Phe}•CO instead of **5^{Bz}•CO** as yellow powder in a 96% yield. Micro crystals of **6^{Phe}** were obtained by diffusion of *n*-hexane into a CH_2Cl_2 solution of the complex. FT-IR (KBr) 1083, and 620 cm^{-1} (ClO_4^-); HRMS (FAB^+): m/z 466.1326, calcd for $C_{28}H_{25}CuN_3$ 466.1344; Anal. Calcd for $[Cu^I(L5^{phe})]ClO_4$ ($C_{28}H_{25}ClCuN_3O_4$): C, 59.36; H, 4.45; N, 7.42%. Found: C, 59.39; H, 4.36; N, 7.20%.

$[Cu^I(L6^{PhePh})]ClO_4$ (6^{PhePh}): Ligand $L6^{PhePh}$ (71.4 mg, 0.15 mmol) was treated with $[Cu^I(CH_3CN)_4]ClO_4$ (47.7 mg, 0.15 mmol) in CH_2Cl_2 (5 mL) under Ar atmosphere in a glovebox. After stirring for 5 min at room temperature, insoluble material was removed by filtration. Addition of ether (100 mL) to the filtrate cause a pale yellow powder to precipitate upon standing for several minutes. The supernatant was then removed by decantation, and the remaining pale yellow solid was washed three times with ether and dried to give complex **6^{PhePh}** in a 93% yield. FT-IR (KBr) 1108, 1090, and 625 cm^{-1} (ClO_4^-); HRMS (FAB^+): m/z 542.1650, calcd for $C_{34}H_{29}CuN_3$ 542.1658; Anal. Calcd for $[Cu^I(L6^{PhePh})]ClO_4$ ($C_{34}H_{29}ClCuN_3O_4$): C, 63.55; H, 4.55; N, 6.54%. Found: C, 63.25; H, 4.52; N, 6.43%.

Product Analysis of the Oxygenation Reactions of 6^{Bz} and 6^{Phe}. Complex **6^{Bz}** (60.0 mg, 0.11 mmol) was dissolved in deaerated acetone (20 mL) under anaerobic conditions, and the solution was exposed to O_2 gas at $-80\,^\circ C$ and stirred for 2 h at the same temperature. Addition of ether (100 mL) to the solution cause a green powder to precipitate upon standing for several minutes. The supernatant was then removed by decantation, and the remaining green solid was washed with ether three times and dried to give bis(μ-hydroxo)dicopper(II) complex **7** in a 68% yield. Micro crystals of **7** were obtained by vapor diffusion of ether into an acetone solution of the complex. FT-IR (KBr) 3538 cm^{-1} (OH), 1093 and 621 cm^{-1} (ClO_4^-); HRMS (FAB^+): m/z 452.1176, calcd for $C_{27}H_{23}CuN_3$ 452.1188; Anal. Calcd for $[(Cu^{II}L6^{Bz})_2(\mu\text{-}OH)_2](ClO_4)_2(CH_3OCH_3)_2(H_2O)$ ($C_{60}H_{62}Cl_2Cu_2N_6O_{13}$): C, 56.60; H, 4.91; N, 6.60%. Found: C, 56.58; H, 4.59; N, 6.64%.

The reaction of **6^{Phe}** was carried out similarly, and the single crystals of product **8**, (μ-hydroxo)(μ-alkoxo)dicopper(II) complex, were obtained in the similar manner. FT-IR (KBr) 3519 cm^{-1} (OH), 1095 and 622 cm^{-1} (ClO_4^-); HRMS (FAB^+): m/z 482.1288, calcd for $C_{28}H_{25}CuN_3O$ 482.1294; Anal. Calcd for $[Cu^{II}_2(L6^{phe})(L6^{phe}\text{-}O)(\mu\text{-}OH)](ClO_4)_2(CH_3OH)(CH_3CH_2OCH_2CH_3)$ ($C_{61}H_{64}Cl_2Cu_2N_6O_{12}$): C, 57.64; H, 5.07; N, 6.61%. Found: C, 57.70; H, 4.85; N, 6.23%.

Isolation of the Modified Ligand in the Reaction of 6^{Phe} with O_2. Complex **6^{Phe}** (52.0 mg, 0.092 mmol) was dissolved in deaerated acetone (15 mL) under anaerobic conditions, and the solution was exposed to O_2 gas at $-80\,^\circ C$ and stirred for 2 h at the same temperature. A mixture of organic materials was obtained after an ordinary work-up treatment of the reaction mixture with an NH_3 aq and following extraction by CH_2Cl_2. Yield of the hydroxylation product was determined to be 73% based on the copper(I) starting material by using an integral ratio in the ^1H NMR spectrum between the methine proton (–C*H*OH–) at δ 4.97 of the hydroxylation product. The hydroxylated ligand $L6^{phe}$-OH was isolated by a silica gel column chromatographic treatment on the mixture of organic material (eluent: AcOEt–MeOH); ^1H NMR (400 Hz, $CDCl_3$) δ 2.95 (1H, dd, $J = 10.0$ and 13.0 Hz, –N–C*H*–CHOH–), 3.11 (1H, dd, $J = 2.6$ and 13.5 Hz, –N–C*H*–CHOH–), 4.18 (2H, d, $J = 15.6$ Hz, –N–C*H*$_2$–), 4.31 (2H, d, $J = 15.6$ Hz, –C*H*$_2$–N–), 4.97 (1H, dd, $J = 2.6$ and 10.0 Hz, –N–CH–C*H*OH), 7.07 (1H, br s), 7.20 (1H, t, $J = 7.2$ Hz), 7.28 (1H, t, $J = 6.8$ Hz), 7.37 (2H, d, $J = 8.0$ Hz), 7.47–7.54 (4H, m), 7.72 (2H, ddd, $J = 1.2$, 6.8, and 8.8 Hz), 7.77 (2H, d, $J = 8.4$ Hz), 8.03 (2H, d, $J = 8.4$), 8.15 (2H, d, $J = 8.4$ Hz); ESI-MS (pos.) $m/z = 420.0$ (M + 1).

X-ray Structure Determination. A single crystal was mounted on a CryoLoop (Hamptom Research Co.) or a glass-fiber. The X-ray crystallographic analyses of **5^{Bz}•CO** were performed on a Rigaku Mercury CCD area detector with graphite monochromated Mo Kα radiation ($\lambda = 0.71070$ Å) controlled by a Windows NT running the CrystalClear software package (Rigaku Corp., 1999). The crystal to detector distance was 34.80 mm. The data were collected at a temperature of $-120\,^\circ C$ to $2\theta_{max}$ of 55°. X-ray diffraction data for **6^{Phe}•CH_3CN**, **3^{Bz}•CO**, **5^{Phe}•CO**, **6^{Bz}•CH_3CN**, **6^{Bz}•CO**, **6^{Phe}•CO**, **6^{Phe}**, **6^{PhePh}**, **7**, and **8** were collected by using a Rigaku RAXIS-RAPID imaging plate area detector with graphite monochromated Mo Kα radiation ($\lambda = 0.71070$ Å) to $2\theta_{max}$ of 55.0°. All data were corrected for Lorentz and polarization effects. All crystallographic calculations were performed by using Crystal Structure software package of the Molecular Structure Corporation [Crystal Structure: Crystal Structure Analysis Package version 3.5.1, Rigaku and Rigaku/MSC (2000–2003)]. The structures were solved by direct methods and refined by the full-matrix least squares using SIR-92[23] or SHELXS97.[24] The non-hydrogen atoms were refined anisotropically and hydrogen atoms were refined using the riding model. Crystallographic data have been deposited with Cambridge Crystallographic Data Centre: Deposition numbers CCDC-610488 for compound **3^{Bz}•CO**, CCDC-610489 for compound **5^{Bz}•CO**, CCDC-610490 for compound **5^{Phe}•CO**, CCDC-610491 for compound **6^{Bz}•CO**, CCDC-610492 for compound **6^{Phe}**, CCDC-610493 for compound **6^{Phe}•CH_3CN**, CCDC-610494 for compound **6^{Phe}•CO**, CCDC-610495 for compound **6^{PhePh}**, CCDC-610496 for compound **7**, and CCDC-610497 for compound **8**. Copies of the data can be obtained free of charge via http://www.ccdc.cam.ac.uk/conts/retrieving.html (or from the Cambridge Crystallographic Data Centre, 12, Union Road, Cambridge, CB2 1EZ, UK; Fax: +44 1223 336033; e-mail: deposit@ccdc.cam.ac.uk).

Kinetic Measurements. Kinetic measurements for the oxygenation reactions of copper(I) complexes **6^{Bz}** and **6^{Phe}** and the decomposition process of the peroxo intermediate derived from **6^{Phe}** were performed using a Hewlett Packard 8453 photo diode array spectrophotometer with a Unisoku thermostated cell holder designed for low-temperature measurements (USP-203, a desired temperature can be fixed within $\pm 0.5\,^\circ C$) in acetone at $-94\,^\circ C$. The second-order rate constants for the formation of Cu_2O_2 intermediates were determined from the slopes of the plots of $(A_0 - A)/\{[\text{Cu-complex}]_0(A - A_\infty)\}$ vs time based on the time courses of the absorption change at λ_{max} due to the intermediates. Pseudo-first-order rate constants for the decomposition processes of the peroxo intermediate of $L6^{Phe}$ were determined from the slopes of the plots of $\ln(A - A_\infty)$ vs time based on the time courses of the absorption change at λ_{max} due to the intermediate.

Results and Discussion

Syntheses and Structural Characterizations of Copper(I) Complexes. In this study, the structure and reactivity of the copper(I) complexes of $L3^{Bz}$, $L4^{Bz}$, $L5^{Bz}$, and $L6^{Bz}$ with a benzyl substituent (R = –CH_2Ph, Chart 1) have been compared in detail in order to give further insights into the steric effects of the metal-binding site of the tridentate ligands. The structure and reactivity of the copper(I) complexes of $L5^{Phe}$, $L6^{Phe}$, and $L6^{PhePh}$ (Phe = –CH_2CH_2Ph; PhePh = –CH_2CHPh_2)

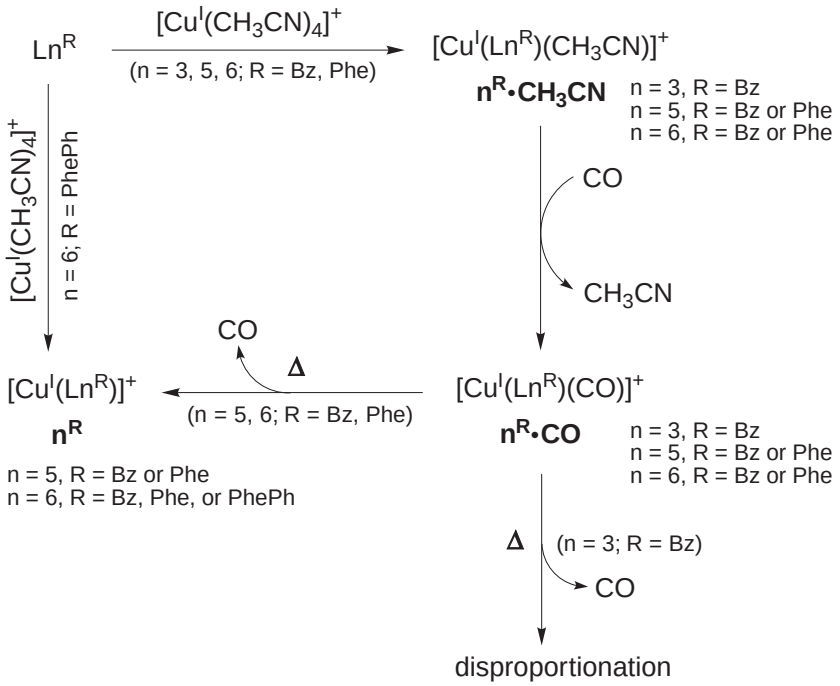

Scheme 1.

have also been examined in order to evaluate the steric effects of the ligand sidearm (R). The synthetic routes of the new copper(I) complexes are summarized in Scheme 1. The syntheses and structures of the copper(I) complexes with $L4^R$ have already been reported.[14]

Treatment of the ligands with an equimolar amount of $[Cu^I(CH_3CN)_4]X$ (X = ClO_4 or PF_6) under anaerobic conditions (Ar) gave the corresponding copper(I) complexes with acetonitrile as a co-ligand, $\boldsymbol{n^R}$**•CH$_3$CN** (n = 3–6, R = Bz or Phe)[25] except for ligand $L6^{PhePh}$ which gave the copper(I) complex $\mathbf{6^{PhePh}}$ without having any ancillary ligands (see Scheme 1). Existence of the CH_3CN molecule in $\boldsymbol{n^R}$**•CH$_3$CN** has been confirmed by ^{1}H NMR and elemental analysis (see, Experimental Section). The crystal structure of $\mathbf{6^{Phe}}$**•CH$_3$CN**, which has a significantly distorted tetrahedral geometry at the metal center is shown in Fig. S1, and the crystallographic data and the selected bond lengths and angles are presented in Tables S1 and S2, respectively. A similar structure was also found for $\mathbf{4^{Bz}}$**•CH$_3$CN**.[14]

The acetonitrile complexes $\boldsymbol{n^R}$**•CH$_3$CN** were then converted to the corresponding CO-complexes $\boldsymbol{n^R}$**•CO** by treating them with CO gas at low temperature.[25] The crystal structures of $\mathbf{3^{Bz}}$**•CO**, $\mathbf{5^{Bz}}$**•CO**, and $\mathbf{6^{Bz}}$**•CO** are shown in Fig. 1. The crystallographic data are listed in Table 1, and the selected bond lengths and angles are summarized in Table 2, in which those of $\mathbf{4^{Bz}}$**•CO** are also included.[14] The crystal structures of $\mathbf{5^{Phe}}$**•CO** and $\mathbf{6^{Phe}}$**•CO** are also presented in Fig. S2, and the crystallographic data and the selected bond lengths and angles are summarized in Tables S3 and S4, respectively. Although all the CO-complexes exhibit a similar structure with significantly distorted tetrahedral geometry with N_3C donor set, comparison of the bond lengths of Cu–$N_{Py(Qu)}$ and Cu–CO among $\boldsymbol{n^{Bz}}$**•CO** (R = Bz) provide some important insights into the steric effects of the hetero-aromatic donor groups (pyridine and quinoline). The average bond lengths Cu–$N_{Py(Qu)}$ between copper(I) ion and the nitrogen atoms of hetero-aromatic donors of the complexes are 2.046 Å ($\mathbf{3^{Bz}}$**•CO**), 2.053 Å ($\mathbf{4^{Bz}}$**•CO**), 2.109 Å ($\mathbf{5^{Bz}}$**•CO**), and 2.041 Å ($\mathbf{6^{Bz}}$**•CO**). Apparently, Cu–N_{Py} bonds in $\mathbf{5^{Bz}}$**•CO** are relatively longer than those of others, indicating that the 6-phenyl substituent on the pyridine donor group imparts a relatively large steric hindrance for the metal binding. Namely, the Cu–N_{Py} bonds in $\mathbf{5^{Bz}}$**•CO** are elongated due to the steric repulsion between the 6-phenyl group and the metal ion. In this respect, the steric effect of the 6-methyl substituent in $\mathbf{4^{Bz}}$**•CO** is not so significant: only a 0.007 Å elongation of Cu–N_{Py} compared to $\mathbf{3^{Bz}}$**•CO**. It should be noted that the bond lengths of Cu–N_{Qu} in $\mathbf{6^{Bz}}$**•CO** are nearly the same as those of $\mathbf{3^{Bz}}$**•CO**, suggesting that the steric effect of the quinoline donor group is the same as that of pyridine in the copper(I) oxidation state. It should be also mentioned that the Cu–CO lengths seem to correlate to the Cu–$N_{Py(Qu)}$ lengths. Namely, the longer the Cu–$N_{Py(Qu)}$, the longer the Cu–CO (Table 2).

The CO ligand can be easily removed from $\boldsymbol{n^R}$**•CO** by heating them in methanol. Thus, $\mathbf{5^R}$**•CO** and $\mathbf{6^R}$**•CO** (R = Bz and Phe) were converted to the corresponding copper(I) complexes without an ancillary ligand, $\mathbf{5^R}$ and $\mathbf{6^R}$, as in the case of the conversion of $\mathbf{4^R}$**•CO** to $\mathbf{4^R}$.[14] In the case of $\mathbf{3^{Bz}}$**•CO** (R = –CH_2Ph), however, removal of the CO ligand caused a rapid disproportionation to give a mixture of a copper(II) complex and copper metal.[10] Thus, the copper(I) complex of $L3^{Bz}$ without any external co-ligand could not be isolated.[26] It is interesting to note that $\mathbf{6^{PhePh}}$ with the large ligand sidearm PhePh (R = –$CH_2CH(Ph)_2$) was directly obtained from the reaction between ligand $L6^{PhePh}$ and $[Cu^I(CH_3CN)_4]ClO_4$ without formation of the corresponding acetonitrile complex as mentioned above. The large substituent PhePh may prohibit the coordination of CH_3CN.

The crystal structures of $\mathbf{6^{Phe}}$ and $\mathbf{6^{PhePh}}$ are shown in Fig. 2.

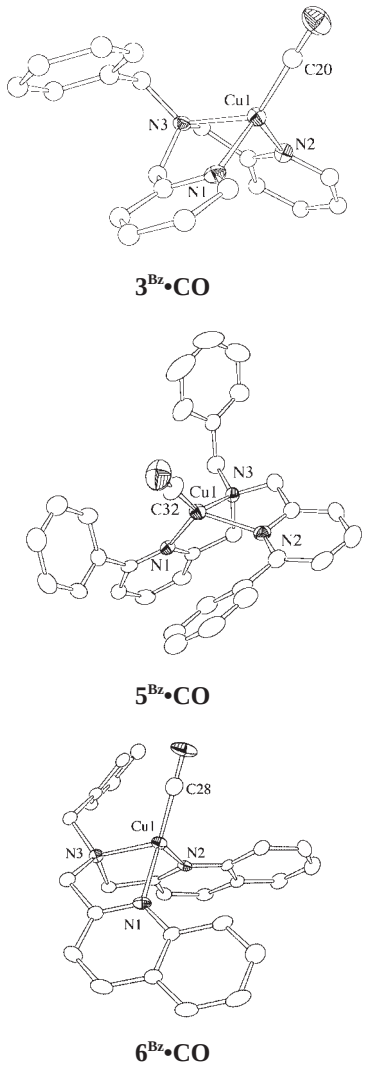

Fig. 1. ORTEP drawings of **3^{Bz}•CO**, **5^{Bz}•CO**, and **6^{Bz}•CO** showing 50% probability thermal ellipsoids. The counter anions and the hydrogen atoms are omitted for clarity.

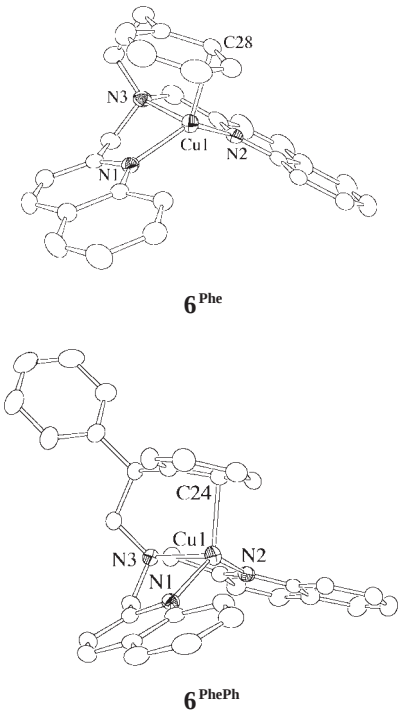

Fig. 2. ORTEP drawings of **6^{Phe}** and **6^{PhePh}** showing 50% probability thermal ellipsoids. The counter anions and the hydrogen atoms are omitted for clarity.

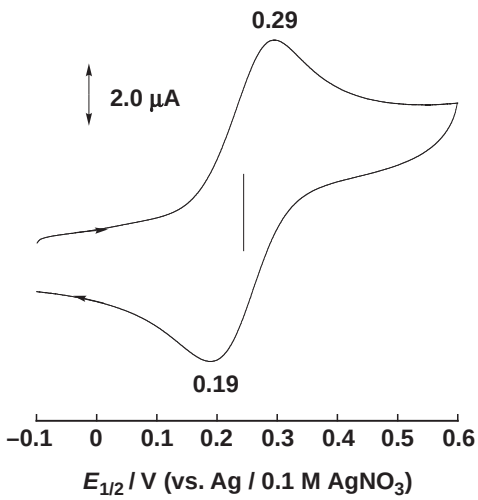

Fig. 3. Cyclic voltammogram of **5^{Bz}•CH$_3$CN** (2.0×10^{-3} M) in CH_3CN containing 0.1 M $TBAPF_6$; working electrode Pt, counter electrode Pt, reference electrode Ag/0.01 M $AgNO_3$, scan rate 50 mV s^{-1}.

The crystallographic data and the selected bond lengths and angles are listed in Tables 1 and 2, respectively. As in the case of **3^{Phe}**,[10,26] **4^{Phe}**,[14] and **4^{PhePh}**,[14] both **6^{Phe}** and **6^{PhePh}** have a significantly distorted trigonal pyramidal geometry involving two nitrogen atoms N(1) and N(2) of the quinoline donor groups and one of the phenyl carbons [C(28) in **6^{Phe}** and C(24) in **6^{PhePh}**] in the basal plane and the tertiary amine nitrogen atom N(3) as the axial ligand. Thus, these complexes also exhibit an interesting d–π interaction with an κC-binding mode between the copper(I) ion and the ortho-carbon atom of the aromatic ring of the ligand sidearm. Although crystal structure of **5^{Phe}** has not been determined, the complex may also have a similar structure with the κC-type d–π interaction.

Oxidation Potential of Copper(I) Complexes. The oxidation potential of the complex is an important indicator of the electron-donor ability of the ligands. Figure 3 shows the cyclic voltammogram of **5^{Bz}•CH$_3$CN** measured in CH_3CN as a typical example. The cyclic voltammograms for the other complexes were measured under the same experimental conditions. In all cases, a reversible or a quasi-reversible Cu^{I}/Cu^{II} redox couple was observed, from which the oxidation potentials ($E_{1/2}$) of the copper(I) complexes were determined as the mid-pint of the oxidation and reduction peak potentials as summarized in Table 3.

As can be seen in Table 3, the $E_{1/2}$ values of **4^{Bz}•CH$_3$CN**, **6^{Bz}•CH$_3$CN**, and **6^{Phe}•CH$_3$CN** are nearly the same (≈0.15 V vs Ag/0.01 M $AgNO_3$), whereas the oxidation potential of **5^{Bz}•CH$_3$CN** is higher. This could be attributed to the steric effect of 6-phenyl group of **5^{Bz}•CH$_3$CN**. Namely, the phenyl group at C-6 on the pyridine ring of L5^{Bz} may induce a larger steric

Table 1. Summary of the X-ray Crystallographic Data of **3^{Bz}·CO**, **5^{Bz}·CO**, **6^{Bz}·CO**, **6^{Phe}**, **6^{PhePh}**, and **8**

	3^{Bz}·CO	**5^{Bz}·CO**	**6^{Bz}·CO**	**6^{Phe}**	**6^{PhePh}**	**8**
Formula	$C_{20}H_{19}N_3CuOPF_6$	$C_{32}H_{27}N_3CuClO_5$	$C_{28}H_{23}N_3CuClO_5$	$C_{28}H_{25}N_3CuClO_4$	$C_{34}H_{29}N_3CuClO_4$	$C_{56}H_{50}N_6Cu_2Cl_2O_{10}$
Formula weight	525.90	632.58	580.51	566.52	642.62	1165.04
Crystal system	orthorhombic	orthorhombic	monoclinic	monoclinic	monoclinic	monoclinic
Space group	*Pna*2$_1$ (#33)	*Pna*2$_1$ (#33)	*P*2$_1$/*n* (#14)	*P*2$_1$/*c* (#14)	*P*2$_1$/*c* (#14)	*P*2$_1$/*c* (#14)
a/Å	9.778(13)	23.389(2)	12.5204(10)	11.971(10)	11.8255(7)	14.039(6)
b/Å	13.900(13)	11.1658(10)	11.7910(10)	16.634(13)	20.2106(13)	29.254(10)
c/Å	16.111(15)	22.239(2)	17.7172(16)	12.628(8)	12.9974(8)	15.386(7)
α/deg	90	90	90	90	90	90
β/deg	90	90	105.410(5)	98.79(3)	112.649(3)	101.617(20)
γ/deg	90	90	90	90	90	90
V/Å^3	2189.7(40)	5808.0(10)	2521.5(4)	2485.0(32)	2866.8(3)	6189.7(41)
Z	4	8	4	4	4	4
F(000)	1064.00	2608.00	1192.00	1168.00	1328.00	2400.00
D_{calcd}/g cm^{-3}	1.595	1.447	1.529	1.514	1.489	1.250
T/K	153	153	153	153	153	153
Crystal size/mm^3	0.20 × 0.20 × 0.10	0.20 × 0.20 × 0.10	0.20 × 0.20 × 0.20	0.40 × 0.40 × 0.40	0.40 × 0.30 × 0.20	0.40 × 0.20 × 0.20
μ (Mo Kα)/cm^{-1}	11.384	8.902	10.176	10.275	9.006	8.292
$2\theta_{max}$/deg	54.9	55.0	55.0	54.9	54.9	55.0
No. of reflns measd	19861	55829	24394	23177	27027	57661
No. of reflns obsd	12203 ([$I > 2.00\sigma(I)$])	40872 ([$I > 3.00\sigma(I)$])	11485 ([$I > 3.00\sigma(I)$])	4446 ([$I > 2.00\sigma(I)$])	5488 ([$I > 2.00\sigma(I)$])	7045 ([$I > 1.00\sigma(I)$])
No. of variables	309	812	367	362	415	747
R[a)]	0.0565	0.0590	0.0420	0.0335	0.0428	0.0864
R_w[b)]	0.0758	0.0640	0.0700	0.0408	0.0664	0.1050
GOF	1.007	1.034	1.079	1.004	0.979	1.008

a) $R = \Sigma||F_o| - |F_c||/\Sigma|F_o|$. b) $R_w = [\Sigma w(|F_o| - |F_c|)^2/\Sigma wF_o^2]^{1/2}$.

Table 2. Selected Bond Lengths (Å) and Angles (°) of $\mathbf{3^{Bz}\cdot CO}$, $\mathbf{4^{Bz}\cdot CO}$, $\mathbf{5^{Bz}\cdot CO}$, $\mathbf{6^{Bz}\cdot CO}$, $\mathbf{6^{Phe}}$, $\mathbf{6^{PhePh}}$, and **8**

$3^{Bz}\cdot CO$

Cu(1)–N(1)	2.059(3)	Cu(1)–N(2)	2.033(2)
Cu(1)–N(3)	2.184(3)	Cu(1)–C(20)	1.799(4)
N(1)–Cu(1)–N(2)	111.28(13)	N(1)–Cu(1)–N(3)	81.90(12)
N(1)–Cu(1)–C(20)	115.73(16)	N(2)–Cu(1)–N(3)	81.39(12)
N(2)–Cu(1)–C(20)	123.99(17)	N(3)–Cu(1)–C(20)	132.9(2)

$4^{Bz}\cdot CO$[a)]

Molecule 1

Cu(1)–N(1)	2.063(3)	Cu(1)–N(2)	2.042(2)
Cu(1)–N(3)	2.131(3)	Cu(1)–C(22)	1.806(3)
N(1)–Cu(1)–N(2)	105.22(9)	N(1)–Cu(1)–N(3)	80.51(10)
N(1)–Cu(1)–C(22)	117.6(1)	N(2)–Cu(1)–N(3)	83.73(9)
N(2)–Cu(1)–C(22)	129.0(1)	N(3)–Cu(1)–C(33)	127.7(1)

Molecule 2

Cu(2)–N(4)	2.051(3)	Cu(2)–N(5)	2.054(3)
Cu(2)–N(6)	2.124(3)	Cu(2)–C(44)	1.800(3)
N(4)–Cu(2)–N(5)	108.0(1)	N(4)–Cu(2)–N(6)	80.6(1)
N(4)–Cu(2)–C(44)	122.2(1)	N(5)–Cu(2)–N(6)	83.68(10)
N(5)–Cu(2)–C(44)	121.8(1)	N(6)–Cu(2)–C(44)	129.0(1)

$5^{Bz}\cdot CO$

Cu(1)–N(1)	2.067(2)	Cu(1)–N(2)	2.150(2)
Cu(1)–N(3)	2.131(2)	Cu(1)–C(32)	1.816(3)
N(1)–Cu(1)–N(2)	115.26(10)	N(1)–Cu(1)–N(3)	81.06(9)
N(1)–Cu(1)–C(32)	126.55(12)	N(2)–Cu(1)–N(3)	78.12(9)
N(2)–Cu(1)–C(32)	106.46(14)	N(3)–Cu(1)–C(32)	141.26(13)

$6^{Bz}\cdot CO$

Cu(1)–N(1)	2.050(2)	Cu(1)–N(2)	2.032(2)
Cu(1)–N(3)	2.108(2)	Cu(1)–C(28)	1.797(3)
N(1)–Cu(1)–N(2)	104.18(10)	N(1)–Cu(1)–N(3)	82.03(11)
N(1)–Cu(1)–C(28)	125.63(14)	N(2)–Cu(1)–N(3)	84.38(11)
N(2)–Cu(1)–C(28)	123.98(12)	N(3)–Cu(1)–C(28)	122.84(14)

6^{Phe}

Cu(1)–N(1)	1.982(15)	Cu(1)–N(2)	1.989(18)
Cu(1)–N(3)	2.212(15)	Cu(1)–C(28)	2.217(2)
N(1)–Cu(1)–N(2)	127.57(6)	N(1)–Cu(1)–N(3)	83.90(6)
N(1)–Cu(1)–C(28)	125.42(8)	N(2)–Cu(1)–N(3)	82.79(6)
N(2)–Cu(1)–C(28)	106.77(7)	N(3)–Cu(1)–C(28)	99.65(6)

6^{PhePh}

Cu(1)–N(1)	1.9953(17)	Cu(1)–N(2)	2.0317(17)
Cu(1)–N(3)	2.2144(18)	Cu(1)–C(24)	2.175(2)
N(1)–Cu(1)–N(2)	124.87(7)	N(1)–Cu(1)–N(3)	83.58(6)
N(1)–Cu(1)–C(24)	131.75(7)	N(2)–Cu(1)–N(3)	81.46(7)
N(2)–Cu(1)–C(24)	102.06(7)	N(3)–Cu(1)–C(24)	93.90(7)

8

Cu(1)–N(1)	2.006(8)	Cu(1)–N(2)	2.047(8)
Cu(1)–N(3)	2.263(7)	Cu(1)–O(5)	1.930(6)
Cu(1)–O(6)	1.941(6)	Cu(2)–O(5)	1.901(6)
Cu(2)–O(6)	1.931(6)	Cu(2)–N(4)	2.190(9)
Cu(2)–N(5)	2.015(7)	Cu(2)–N(6)	2.003(8)
Cu(1)–Cu(2)	2.937(16)	O(5)–O(6)	2.449(9)
O(5)–Cu(1)–O(6)	78.5(2)	O(5)–Cu(1)–N(1)	90.9(3)
O(5)–Cu(1)–N(2)	174.2(3)	O(5)–Cu(1)–N(3)	105.2(2)
O(6)–Cu(1)–N(1)	166.8(3)	O(6)–Cu(1)–N(2)	98.3(3)
O(6)–Cu(1)–N(3)	109.7(2)	N(1)–Cu(1)–N(2)	91.6(3)
N(1)–Cu(1)–N(3)	80.5(3)	N(2)–Cu(1)–N(3)	80.4(2)
O(5)–Cu(2)–O(6)	79.4(2)	O(5)–Cu(2)–N(4)	112.1(3)
O(5)–Cu(2)–N(5)	106.4(3)	O(5)–Cu(2)–N(6)	162.4(3)
O(6)–Cu(2)–N(4)	106.3(3)	N(4)–Cu(2)–N(5)	102.1(3)
O(6)–Cu(2)–N(6)	85.7(2)	N(5)–Cu(2)–N(6)	81.1(3)
N(4)–Cu(2)–N(6)	80.9(3)	O(6)–Cu(2)–N(5)	146.2(3)

a) Data are taken from Ref. 14.

repulsion between the substituent and the metal ion, thus weakening the coordinative interaction. This will decrease the electron-donation from the pyridine nitrogen, causing the increase of the oxidation potential of copper(I). In fact, Cu–N_{Py} bonds in **5^{Bz}•CO** (av. 2.109 Å) are longer than those of the others as discussed above. On the other hand, the very negative $E_{1/2}$ value of **3^{Bz}•CH_3CN** (−0.14 V) can be attributed to the stronger electron-donor ability of $L3^R$ ligand as previously reported.[10]

Reaction of Copper(I) Complexes and O_2. As mentioned in the Introduction, the copper(I) complex supported by ligand $L3^{Phe}$ (**3^{Phe}**, R = –CH_2CH_2Ph) has been shown to react readily with O_2 at low temperature (−94 °C) to give the bis(μ-oxo)dicopper(III) complex **B**.[10] It has also been shown that introduction of a methyl group at C-6 of the pyridine nucleus of the bis(2-pyridylmethyl)amine tridentate $L3^R$-type ligands to give $L4^R$ resulted in a decrease of the electron-donor ability of pyridine nitrogen to afford the side-on peroxodicopper(II) complex **A**.[14] In this case, the O–O bond of peroxo complex **A** supported by $L4^R$ was found to be weaker ($\nu_{O-O} \cong 720$ cm^{-1}) than that of the peroxo complex involving $L1^R$ ($\nu_{O-O} \cong 745\,cm^{-1}$).[14]

In order to give further insights into the steric effects of the C-6 substituents of pyridine on copper(I)/O_2-reactivity, the oxygenation reactions of **5^{Bz}** and **5^{Phe}**, which have the larger 6-phenyl group on the pyridine moiety, were examined under the same experimental conditions. However, these compounds showed virtually no reactivity toward O_2. This could be attributed in part to their higher redox potential, stabilizing the copper(I) oxidation sate (see Table 3). The large 6-phenyl groups of $L5^R$ may also prevent the approach of O_2 to the copper(I) center, prohibiting the oxygenation reaction.

Table 3. Oxidation Potentials of the Copper(I) Complexes in CH_3CN[a)]

Complex	$E_{1/2}$/V vs Ag/0.01 M $AgNO_3$
3^{Bz}•CH_3CN	−0.14
4^{Bz}•CH_3CN	0.15
5^{Bz}•CH_3CN	0.24
6^{Bz}•CH_3CN	0.16
6^{Phe}•CH_3CN	0.15

a) In CH_3CN containing 0.1 M $TBAPF_6$; working electrode Pt, counter electrode Pt, and reference electrode Ag/0.01 M $AgNO_3$.

On the other hand, copper(I) complexes **6^{Bz}** and **$6a^{Phe}$** exhibited relatively high reactivity toward O_2 at low temperature (−94 °C). Figure 4 shows the spectral change upon introduction of O_2 gas into an acetone solution of **6^{Bz}**. The absorption bands at 362, 394, ≈460 (shoulder), and 535 nm gradually increased as the reaction proceeded. The absorption bands at 362 and 535 nm were attributed to a (μ-η^2:η^2-peroxo)dicopper(II) complex **A**, and the band at 394 nm was due to the formation of the bis(μ-oxo)dicopper(III) species **B**.[3,4,27] This was confirmed by resonance Raman spectroscopy, Fig. 5. When the reaction solution of **6^{Bz}** with $^{16}O_2$ was excited with 406.7 nm

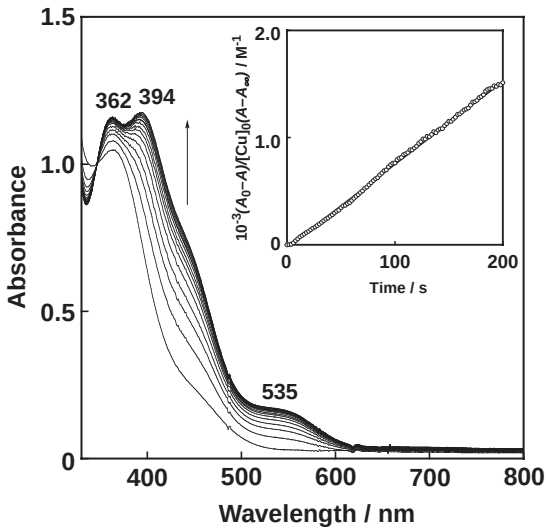

Fig. 4. Spectral change observed upon introduction of O_2 gas into an acetone solution of **6^{Bz}** (2.0×10^{-3} M) at −94 °C in a 1 mm path length UV cell. Inset: second-order plot based on the absorption change at 400 nm.

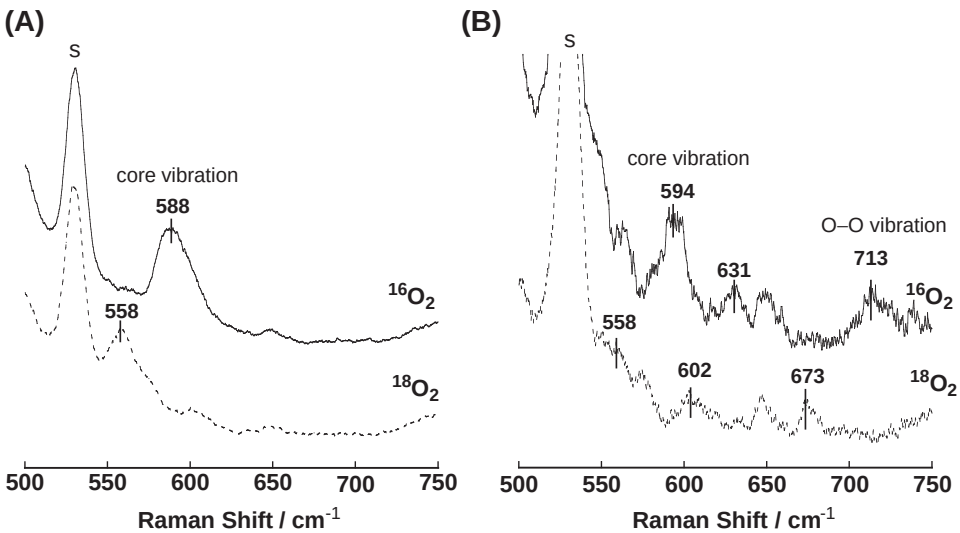

Fig. 5. Resonance Raman spectra of the reaction solution of **6^{Bz}** with $^{16}O_2$ (solid line) and with $^{18}O_2$ (dashed line) obtained with an excitation wavelength of (A) 406.7 nm and (B) 514.5 nm in acetone at −90 °C.

laser light, an intense Raman band was observed at 588 cm^{-1} that shifted to 558 cm^{-1} upon $^{18}O_2$ substitution (Fig. 5A). The peak position at 588 cm^{-1} and its isotope shift of 30 cm^{-1} are within the range of those of the reported bis(μ-oxo)dicopper(III) complexes (Cu_2O_2 core breathing vibration involving Cu–O stretching).[27,28] On the other hand, the Raman spectrum obtained by excitation with 514.5 nm laser light gave a new band at 713 cm^{-1} that shifted to 673 cm^{-1} with $^{18}O_2$ (Fig. 5B). The peak at 713 cm^{-1} and its isotope shift of 40 cm^{-1} are consistent with the formation of (μ-η^2:η^2-peroxo)dicopper(II) complex (O–O stretching vibration).[29] It should be noted here that there is an additional isotope sensitive Raman band at 631 cm^{-1} that shifted to 602 cm^{-1} (Fig. 5B). Judging from the peak position and its isotope shift (29 cm^{-1}), these bands could also be assigned to an isomeric form of the bis(μ-oxo)dicopper(III) species; however, definitive assignment of these bands requires further experiments. It should be also mentioned that the O–O bond stretching vibration of the (μ-η^2:η^2-peroxo)dicopper(II) complex with $L6^{Bz}$ (713 cm^{-1}) is nearly identical to that of the peroxo complex with $L4^{Bz}$ (714 cm^{-1}), but significantly lower than that of the $L1^{Bz}$-peroxo complex (745 cm^{-1}), demonstrating that the O–O bond of **A** in the $L6^{Bz}$-system is also weaker than that in the $L1^{Bz}$-system.

In the case of $\mathbf{6^{Phe}}$, the reaction was much simpler as shown in Fig. 6. In this case, the major product was the (μ-η^2:η^2-peroxo)dicopper(II) complex **A** which has an intense absorption band at 360 nm together with a small band at 515 nm, which are the characteristic LMCT bands of the side-on peroxodicopper(II) complex.[29] In this case, the resonance Raman spectra showed two distinct bands at 737 and 724 cm^{-1} that shifted to one band at 692 cm^{-1} upon $^{18}O_2$-substituion (Fig. S4). The Raman bands at 737 and 724 cm^{-1} could be assigned to a Fermi doublet of the O–O bond stretching vibration, since the isotope shift of 39 cm^{-1} obtained by subtracting the frequency (692 cm^{-1}) of the ^{18}O-derivative from the average frequency (731 cm^{-1}) of the ^{16}O-derivaitve agrees with the isotope shift reported for the side-on peroxodicopper(II) complexes **A** (38–43 cm^{-1}).[3] The larger alkyl substituent (R = Phe = $-CH_2CH_2Ph$) in the $L6^{Phe}$-complex may prevent the two copper ions from approaching closer (≈2.8 Å), which is required for the formation of the bis(μ-oxo)dicopper(III) complex **B**, thus providing the peroxo complex **A** (typical Cu–Cu distance ≈3.6 Å) as the major product. This, on the other hand, would make the O–O bond stronger in the $L6^{Phe}$ complex as compared to the $L6^{Bz}$ complex (ν_{O-O} = 731 cm^{-1} of the $L6^{Phe}$ complex vs ν_{O-O} = 713 cm^{-1} of the $L6^{Bz}$ complex).

For both $\mathbf{6^{Bz}}$ and $\mathbf{6^{Phe}}$, the formation of Cu_2/O_2 intermediates obeyed second-order kinetics as shown in the insets of Figs. 4 and 6, and the second-order rate constants were 7.7 and 44.7 $M^{-1}\,s^{-1}$, respectively. This suggests that the initial formation of a 1:1 adduct between the copper(I) complex and O_2 is in a fast equilibrium, and the subsequent reaction of the mononuclear copper–dioxygen adduct, which is probably a side-on superoxocopper(II) complex **C**[30] and another molecule of the copper(I) complex to form the (μ-η^2:η^2-peroxo)dicopper(II) complex **A** is the rate-determining step (Scheme 2). It has been reported that the energy levels of the (μ-η^2:η^2-peroxo)dicopper(II) complex **A** and the bis(μ-oxo)dicopper(III) complex **B** are very close, and the equilibrium position between **A** and **B** is easily altered by the solvent, the counter anion, and the steric and/or electronic effects of the supporting ligands.[27] Thus, for the present system with $L6^R$, the equilibrium position between **A** and **B** was affected by the steric bulkiness of the ligand sidearm R (Bz vs Phe) as demonstrated in Figs. 4 and 6. Overall, the reactivity of $\mathbf{6^{Phe}}$ toward O_2 is close to that of $\mathbf{4^R}$.

It should be noted that $\mathbf{6^{PhePh}}$ having the largest alkyl substituent ($-CH_2CHPh_2$) had virtually no reactivity toward O_2

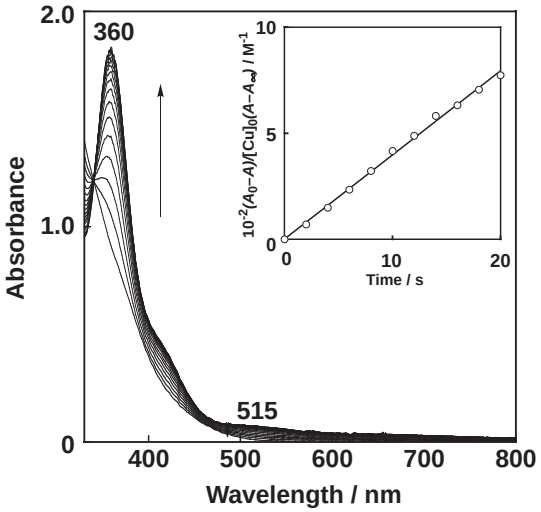

Fig. 6. Spectral change observed upon introduction of O_2 gas into an acetone solution of $\mathbf{6^{Phe}}$ (2.0×10^{-3} M) at −94 °C in a 1 mm path length UV cell. Inset: second-order plot based on the absorption change at 360 nm.

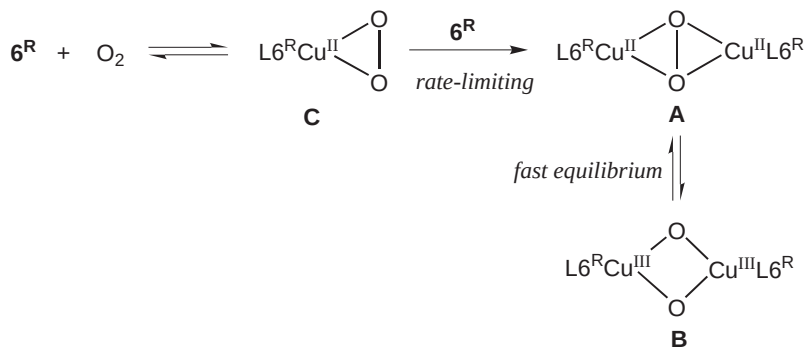

Scheme 2.

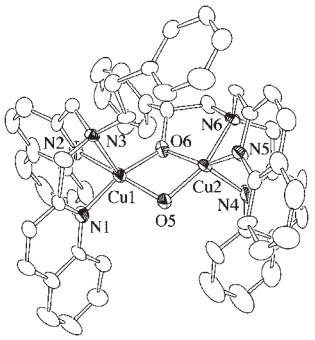

Fig. 7. ORTEP drawing of $[(L6^{Phe\text{-}O})(L6^{Phe})Cu^{II}_2(\mu\text{-}OH)](ClO_4)_2$ (**8**) showing 30% probability thermal ellipsoids. The counter anions and the hydrogen atoms are omitted for clarity.

at low temperature. This is due to the strong d–π interaction between the copper(I) ion and the phenyl group of $-CH_2-CHPh_2$ (see, Fig. 2) as in the case of $\mathbf{1}^{\mathbf{PhePh}}$.[31]

The Cu_2/O_2 complexes (**A** and **B**) supported by $L6^R$ (R = Bz and Phe) gradually decomposed even at low temperature to give different dicopper(II) products. In the case of $L6^{Bz}$, a bis(μ-hydroxo)dicopper(II) complex, $[L6^{Bz}{}_2Cu^{II}_2(\mu\text{-}OH)_2](ClO_4)_2\cdot(CH_3)_2CO$ (**7**), was isolated as the decomposition product in a 68% yield as shown in Fig. S3.[32] Although mechanistic details for the formation of bis(μ-hydroxo)dicopper(II) complex have yet to be determined fully, this is a common product of the decomposition reaction of Cu_2/O_2 species.[4] The complex has a center of symmetry at the center of the Cu_2O_2 core, and the copper(II) center has a distorted square pyramidal structure ($\tau = 0.156$)[33] consisting of quinoline nitrogen N(2), tertiary amine nitrogen N(3), two oxygen atoms of the hydroxo bridges O(6) and O*(6) at the equatorial positions and another quinoline nitrogen N(1) as the axial ligand. The axial ligands coordinate to the copper ions in an anti-conformation. The X-ray crystallographic data and selected bond lengths and angles are listed in Tables S5 and S6, respectively.

In the case of $L6^{Phe}$, on the other hand, ligand hydroxylation occurred at one of the benzylic positions of the phenethyl group (Phe) to give a (μ-alkoxo)(μ-hydroxo)dicopper(II) complex, $[(L6^{Phe\text{-}O})(L6^{Phe})Cu^{II}_2(\mu\text{-}OH)](ClO_4)_2$ (**8**), in a 73% yield. The crystal structure of the dicopper(II) product is shown in Fig. 7, and the X-ray crystallographic data and the selected bond lengths and angles are summarized in Tables 1 and 2, respectively. The Cu(1) center has a distorted square pyramidal structure ($\tau = 0.123$) consisting of two quinoline nitrogen atoms N(1) and N(2), oxygen atom of the bridging OH group O(5), and alkoxy oxygen O(6) of the modified ligand sidearm $L6^{Phe\text{-}OH}$ (Chart 3) in the equatorial plane and tertiary amine nitrogen atom N(3) at the axial position. The Cu(2) center also has a distorted square pyramidal geometry ($\tau = 0.27$) involving quinoline nitrogen atom N(5), tertiary amine nitrogen atom N(6), oxygen atom of the bridging OH group O(5), and alkoxy oxygen O(6) in the equatorial plane and quinoline nitrogen N(4) occupying the axial position. Benzylic hydroxylation was unambiguously confirmed by the X-ray structure of **8**. Aliphatic ligands have been shown to undergo hydroxylation in Cu_2/O_2 systems.[34–36]

Figure 8 shows the spectral change for the aliphatic ligand

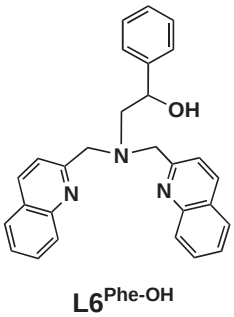

$L6^{Phe\text{-}OH}$

Chart 3.

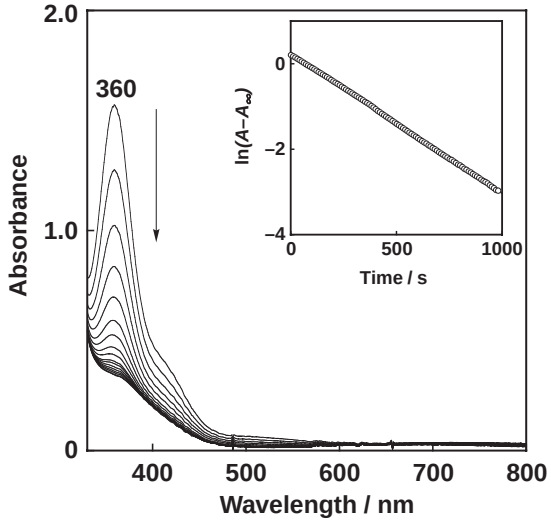

Fig. 8. Spectral change for the aliphatic ligand hydroxylation reaction in the $L6^{Phe}$ system in acetone at $-94\,^{\circ}C$. Inset: first-order plot based on the absorption change at 360 nm.

hydroxylation reaction. As shown in the inset of Fig. 8, the reaction obeys first-order kinetics, suggesting that the ligand hydroxylation is a unimolecular (intramolecular) process at the Cu_2O_2 core. From the slope of the first-order plot, the first-order rate constant k was obtained. The temperature-dependence of the first-order rate constant k (Eyring Plot) was also examined as shown in Fig. 9, from which the activation parameters of the reaction were obtained as $\Delta H^{\ddagger} = 20.3 \pm 0.6\,kJ\,mol^{-1}$ and $\Delta S^{\ddagger} = -175 \pm 3.0\,J\,K^{-1}\,mol^{-1}$. The activation parameters $\Delta H^{\ddagger}$ and $\Delta S^{\ddagger}$ of the present reaction are fairly close to those of the reported for the aliphatic ligand hydroxylation reaction of $\mathbf{1}^{\mathbf{Phe}}$ by O_2 ($\Delta H^{\ddagger} = 28.1 \pm 1.0\,kJ\,mol^{-1}$, $\Delta S^{\ddagger} = -155 \pm 5\,J\,K^{-1}\,mol^{-1}$),[34] suggesting a similar reaction mechanism. Namely, the active oxygen species in this reaction may also be a bis(μ-oxo)dicopper(III) **B** generated by the O–O bond homolysis of (μ-η^2:η^2-peroxo)dicopper(II) **A** as in the case of the $\mathbf{1}^{\mathbf{Phe}}$ system,[34] and aliphatic C–H bond hydroxylation may involve hydrogen-atom abstraction followed by an oxygen rebound mechanism or its concerted variant as previously reported.[35,36]

Summary

We have been investigating the ligand effects on the structure and O_2-reactivity of the copper(I) complexes using a

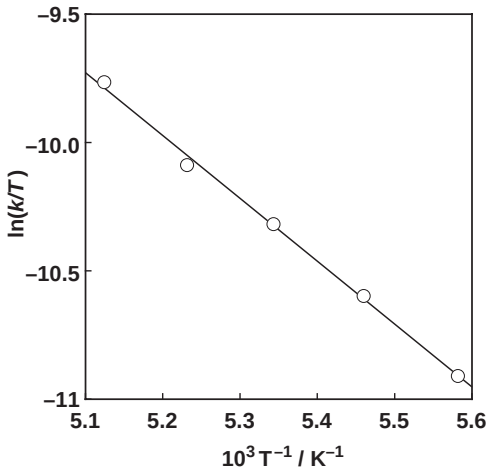

Fig. 9. Eyring plot for the aliphatic ligand hydroxylation of the peroxo intermediate supported by $L6^{Phe}$ in acetone.

series of tridentate ligands shown in Chart 1. In this study, steric effects of the hetero-aromatic donor groups have been examined using bis[(6-phenyl-2-pyridyl)methyl]amine tridentate ligands $L5^R$ and bis(2-quinolylmethyl)amine tridentate ligands $L6^R$.

Unexpectedly, the 6-phenyl group of $L5^R$ had a significantly large steric effect on the reactivity of copper(I) complexes toward O_2. In other words, the copper(I) complexes $\mathbf{5^R}$ completely lost their O_2-reactivity in contrast to the high O_2-reactivity of $\mathbf{3^{Phe}}$ and $\mathbf{4^R}$, which gave the bis(μ-oxo)dicopper(III) complex **B** and the (μ-η^2:η^2-peroxo)dicopper(II) complex **A**, respectively.[10,14] This was attributed to the higher oxidation potential of $\mathbf{5^R}$, stabilizing the copper(I) oxidation sate (see Table 3) as well as the large steric effect of the 6-phenyl groups preventing the approach of O_2 to the copper(I) reaction center.

Judging from the structure and reactivity, $L6^R$ has been found to exhibit similar ligand effects as those of $L4^R$. Thus, $\mathbf{6^R}$ smoothly reacted with O_2 to give the (μ-η^2:η^2-peroxo)-dicopper(II) complex **A** and the bis(μ-oxo)dicopper(III) complex **B**, and the product ratio of these two complexes was largely affected by subtle modification of the ligand sidearm (R; Bz vs Phe). The Cu_2O_2 intermediate supported by $L6^{Phe}$ induced aliphatic ligand hydroxylation, for which hydrogen atom abstraction and oxygen rebound mechanism or its concerted variant was suggested similar to related aliphatic ligand hydroxylation reactions.[34–36] The reaction will provide important insights into the catalytic mechanism of pMMO (particulate methane monooxygenase).[37]

This work was financially supported in part by Grants-in-Aid for Scientific Research (Nos. 17350086, 18037062, and 18033045) from the Ministry of Education, Culture, Sports, Science and Technology, Japan.

Supporting Information

ORTEP drawings (Figs. S1–S3), summary of X-ray crystallographic data (Tables S1, S3, and S5), and selected bond lengths and angles (Tables S2, S4, and S6) of complexes $\mathbf{6^{Phe}}$•$\mathbf{CH_3CN}$, $\mathbf{5^{Phe}}$•**CO**, $\mathbf{5^{Phe}}$•**CO**, and **7** and the resonance Raman spectra of the (μ-η^2:η^2-peroxo)dicopper(II) complex of $L6^{Phe}$ (Fig. S4). These materials are available free of charge on the Web at: http://www.csj.jp/journals/bcsj/.

References

1 S. Itoh, S. Fukuzumi, *Bull. Chem. Soc. Jpn.* **2002**, *75*, 2081.
2 K. D. Karlin, S. Kaderli, A. D. Zuberbuhler, *Acc. Chem. Res.* **1997**, *30*, 139.
3 L. M. Mirica, X. Ottenwaelder, T. D. P. Stack, *Chem. Rev.* **2004**, *104*, 1013.
4 E. A. Lewis, W. B. Tolman, *Chem. Rev.* **2004**, *104*, 1047.
5 K. D. Karlin, M. S. Haka, R. W. Cruse, G. J. Meyer, A. Farooq, Y. Gultneh, J. C. Hayes, J. Zubieta, *J. Am. Chem. Soc.* **1988**, *110*, 1196.
6 K. D. Karlin, J. C. Hayes, Y. Gultneh, R. W. Cruse, J. W. McKown, J. P. Hutchinson, J. Zubieta, *J. Am. Chem. Soc.* **1984**, *106*, 2121.
7 E. Pidcock, H. V. Obias, M. Abe, H. C. Liang, K. D. Karlin, E. I. Solomon, *J. Am. Chem. Soc.* **1999**, *121*, 1299.
8 E. Pidcock, H. V. Obias, C. X. Zhang, K. D. Karlin, E. I. Solomon, *J. Am. Chem. Soc.* **1998**, *120*, 7841.
9 S. Itoh, H. Kumei, M. Taki, S. Nagatomo, T. Kitagawa, S. Fukuzumi, *J. Am. Chem. Soc.* **2001**, *123*, 6708.
10 T. Osako, Y. Ueno, Y. Tachi, S. Itoh, *Inorg. Chem.* **2003**, *42*, 8087.
11 K. D. Karlin, S. E. Sherman, *Inorg. Chim. Acta* **1982**, *65*, L39.
12 H. Nagao, N. Komeda, M. Mukaida, M. Suzuki, K. Tanaka, *Inorg. Chem.* **1996**, *35*, 6809.
13 T. Osako, Y. Tachi, M. Taki, S. Fukuzumi, S. Itoh, *Inorg. Chem.* **2001**, *40*, 6604.
14 T. Osako, S. Terada, T. Tosha, S. Nagatomo, H. Furuuchi, S. Fujinami, T. Kitagawa, M. Suzuki, S. Itoh, *Dalton Trans.* **2005**, 3514.
15 N. Wei, N. N. Murthy, K. D. Karlin, *Inorg. Chem.* **1994**, *33*, 6093.
16 K. D. Karlin, N. Wei, B. Jung, S. Kaderli, P. Niklaus, A. D. Zuberbühler, *J. Am. Chem. Soc.* **1993**, *115*, 9506.
17 C.-I. Chuang, K. Lim, Q. Chen, J. Zubieta, J. W. Canary, *Inorg. Chem.* **1995**, *34*, 2562.
18 D. D. Perrin, W. L. F. Armarego, D. R. Perrin, *Purification of Laboratory Chemicals*, 4th ed., Pergamon Press, Elmsford, NY, **1996**.
19 B. d. Bruin, M. J. Boerakker, J. A. Brands, J. J. J. M. Donners, M. P. J. Donners, R. d. Gelder, J. M. M. Smits, A. W. Gal, A. L. Spek, *Chem. Eur. J.* **1999**, *5*, 2921.
20 S. V. Kryatov, S. Taktak, I. V. Korendovych, E. V. Rybak-Akimova, J. Kaizer, S. Torelli, X. Shan, S. Mandal, V. L. MacMurdo, A. M. i. Payeras, L. Que, Jr., *Inorg. Chem.* **2005**, *44*, 85.
21 T. Osako, S. Nagatomo, T. Kitagawa, C. J. Cramer, S. Itoh, *J. Biol. Inorg. Chem.* **2005**, *10*, 581.
22 Z. He, D. C. Craig, S. B. Colbran, *J. Chem. Soc., Dalton Trans.* **2002**, 4224.
23 A. Altomare, G. Cascarano, C. Giacovazzo, A. Guagliardi, M. C. Burla, G. Polidori, M. Camalli, *J. Appl. Crystallogr.* **1994**, *27*, 435.
24 G. M. Sheldrick, *SHELXS-97, Program for the Solution of Crystal Structures*, University of Göttingen, Germany, **1997**.
25 The syntheses and structures of $\mathbf{4^{Bz}}$•$\mathbf{CH_3CN}$ and $\mathbf{4^{Bz}}$•**CO** have already been reported elsewhere.[14]

26 Copper(I) complex **3^{Phe}** of ligand L3^{Phe} (R = –CH_2-CH_2Ph) could be isolated because it is stabilized by an intramolecular d–π interaction.[10]

27 L. Que, Jr., W. B. Tolman, *Angew. Chem., Int. Ed.* **2002**, *41*, 1114.

28 P. L. Holland, C. J. Cramer, E. C. Wilkinson, S. Mahapatra, K. R. Rogers, S. Itoh, M. Taki, S. Fukuzumi, Jr., L. Que, W. B. Tolman, *J. Am. Chem. Soc.* **2000**, *122*, 792.

29 M. J. Baldwin, D. E. Root, J. E. Pate, K. Fujisawa, N. Kitajima, E. I. Solomon, *J. Am. Chem. Soc.* **1992**, *114*, 10421.

30 The mononuclear Cu–O_2 adducts (both Cu^{II}–superoxo and Cu^{III}–peroxo types) with didentate and tridentate supporting ligands have been shown to exhibit a side-on binding.[3]

31 T. Osako, Y. Tachi, M. Doe, M. Shiro, K. Ohkubo, S. Fukuzumi, S. Itoh, *Chem. Eur. J.* **2004**, *10*, 237.

32 Benzaldehyde was obtained as an *N*-dealkylation product in a 11% yield based on the Cu_2O_2 intermediates.

33 A. W. Addison, T. N. Rao, J. Reedijk, J. von Rijn, G. C. Verschoor, *J. Chem. Soc., Dalton Trans.* **1984**, 1349.

34 S. Itoh, H. Nakao, L. M. Berreau, T. Kondo, M. Komatsu, S. Fukuzumi, *J. Am. Chem. Soc.* **1998**, *120*, 2890.

35 S. Itoh, M. Taki, H. Nakao, P. L. Holland, W. B. Tolman, Jr., L. Que, S. Fukuzumi, *Angew. Chem., Int. Ed.* **2000**, *39*, 398.

36 S. Mahapatra, J. A. Halfen, W. B. Tolman, *J. Am. Chem. Soc.* **1996**, *118*, 11575.

37 R. L. Lieberman, A. Rosenzweig, *Nature* **2005**, *434*, 177.